Materials Today Communications 39 (2024) 108875

Contents lists available at ScienceDirect

Materials Today Communications

journal homepage: www.elsevier.com/locate/mtcomm

Sustainable highly stretchable and tough gelatin-alkali lignin hydrogels for scaffolding and 3D printing applications

Guy Decante [a,b], Ibrahim Fatih Cengiz [a,b], João B. Costa [a,b], Maurice N. Collins [c,d], Rui L. Reis [a,b], Joana Silva-Correia [a,b,*], J. Miguel Oliveira [a,b,*]

[a] 3B's Research Group, I3Bs – Research Institute on Biomaterials, Biodegradables and Biomimetics, University of Minho, Headquarters of the European Institute of Excellence on Tissue Engineering and Regenerative Medicine, AvePark, Zona Industrial da Gandra, Barco, Guimarães 4805-017, Portugal
[b] ICVS/3B's - PT Government Associate Laboratory, Braga, Guimarães, Portugal
[c] Bernal Institute, School of Engineering, University of Limerick, Ireland
[d] Health Research Institute, University of Limerick, Ireland

ARTICLE INFO

Keywords:
3D printing
Sustainable biomaterials
Alkali lignin
Hydrogel
Tissue engineering

ABSTRACT

Hydrogels and bioinks obtained from gelatin (Gel) generally present poor mechanical properties and require a series of time-consuming and stepwise chemical processes to exhibit improved elasticity and resistance to fatigue. Alkali lignin (AL) is an underutilized by-product of the paper and pulp industry. It is a widely available and inexpensive biomaterial that presents enormous potential for high-value applications owing to its ease of chemical modification and unique naturally occurring polyaromatic structure. This work aims to develop different GelAL hydrogel formulations with a single-step method that are innovative and sustainable. The results obtained from the mechanical, rheological, and degradation studies of the developed GelAL hydrogels demonstrated that their properties can be easily modified and tuned using straightforward processing techniques, allowing these stretchable and tough hydrogels to be used as bioinks in 3D printing. The modulation of mechanical properties through hydrogel formulations is a result of interactions between the Gel and AL which can be associated with the interplay of anionic sulfonates in AL and the arginine and lysine residues from Gel. The tensile stress at the break for the Gel20AL10 formulation was 32% higher than the value for Gel20AL5 and 157% higher than that of Gel10AL10. The elongation at break also decreased as it averaged 659 ± 149% for the Gel20AL10 formulation, which is 20% more than that of Gel20AL5 and 55% more than the average elongation at break of Gel10AL10. Further zeta potential measurements and quartz crystal microbalance with energy dissipation studies demonstrated that Gel and AL seem to form neutral complexes when mixed. These assays support the idea that AL and Gel are readily bound through weak interactions, and chemical crosslinking strategies need to be considered when degradability and mechanical properties tuning are envisioned. Altogether, these high-performance GelAL hydrogels display mechanical properties similar to soft tissues with high elasticity beyond that of natural hydrogels and fulfill the requirements of a broad range of biomedical and tissue engineering scaffolding applications.

1. Introduction

Current research in polymeric scaffolds and hydrogels [1,2] used in biomedical applications leans towards the development of biocompatible materials with highly controllable properties and easy processability for patient- and application-specific design [3]. These properties include mechanical strength and degradation kinetics, which allow the production of medical devices that can be implanted within patients' bodies for predefined periods of time, while providing adequate mechanical support and/or delivering therapeutics in a controlled manner. Together with the use of 3D models obtained from medical images, 3D printing enables the production of patient-specific tissue engineering scaffolds [4,5]. Sustainability is an important aspect [6,7], and the development of sustainable [8–10] and smart hydrogels/bioinks [11–13], as well as sustainable photoinitiators [14] are trending. Modulation of 3D printability and mechanical properties to align with the

* Corresponding authors at: 3B's Research Group, I3Bs – Research Institute on Biomaterials, Biodegradables and Biomimetics, University of Minho, Headquarters of the European Institute of Excellence on Tissue Engineering and Regenerative Medicine, AvePark, Zona Industrial da Gandra, Barco, Guimarães 4805-017, Portugal.
E-mail addresses: joana.correia@i3bs.uminho.pt (J. Silva-Correia), miguel.oliveira@i3bs.uminho.pt (J.M. Oliveira).

https://doi.org/10.1016/j.mtcomm.2024.108875
Received 8 January 2024; Received in revised form 26 March 2024; Accepted 7 April 2024
Available online 8 April 2024
2352-4928/© 2024 The Authors. Published by Elsevier Ltd. This is an open access article under the CC BY-NC-ND license (http://creativecommons.org/licenses/by-nc-nd/4.0/).

final application is of critical importance. These features are influenced by a range of properties of the hydrogel such as the crosslinking mechanism and rheological characteristics [15,16].

Despite the large array of biomaterials being investigated for tissue engineering and regenerative medicine applications, so far, only a few of them have demonstrated to present both excellent mechanical and biological properties. In particular, gelatin (Gel), a well-known and widely used biomaterial in tissue engineering needs to be crosslinked since it presents considerable limitations in terms of mechanical properties and degradation [17,18]. Lignin [19] is one of the three main constituents of the cell walls of lignocellulosic plants, along with cellulose and hemicellulose. It represents 20–25% of the mass of hardwood and up to 30% of the mass of softwood [20]. Altogether, lignin accounts for approximately 30% of all the organic carbon in the biosphere and as such, it is the most abundant natural polyphenol and the second most abundant biopolymer after cellulose [21]. It acts as a matrix material for polysaccharides, micro-fibrils, and fibers and provides strength to plant stems. It is a three-dimensional, highly heterogenous structure synthesized via enzymatic dehydrogenation of p-coumaryl, coniferyl, and sinapyl alcohols, and the random branching through C-O and C-C bonds of phenoxyl radicals generated from the three monolignols, also called H, G and S units respectively [22]. Moreover, its structure may include additional components such as hydroxycinnamic acids and flavonoids [22]. Lignin displays high functionality thanks to its many different functional groups which include hydroxyls, carboxyls, carbonyls, and methoxyls, allowing lignin to be extensively modified and crosslinked through various chemistries [23]. The relative amounts of these compounds depend on the source of lignin [21]. It is generally accepted that softwoods are rich in G units, hardwoods are rich in G and S units, and grasses are rich in all three units [24].

As a biopolymer, lignin benefits from inherent biocompatibility and biodegradability. While lignin is being used as a green filler in industrial applications, it has also been recently studied for biomedical applications [25]. Additionally, its polyphenolic nature and high anti-oxidant activity may allow for direct neutralization of harmful free radicals and reactive oxygen species, and provide favorable features for the management of chronic wounds and diseases [26,27].

Lignin is widely used in the wood and paper industries. To manufacture paper and board, lignin can be removed from cellulose using chemical pulping processes [28]. One of these processes is the Kraft pulping process, which produces an estimated 70 million tons of Kraft lignin, also named alkali lignin (AL), per year worldwide [29]. However, around 98% of this lignin remains under-utilized, mainly burnt as a low-grade burning fuel or simply discarded [30]. Given its various properties and very high abundance, AL could be an inexpensive and sustainable multifunctional material to be used in numerous other high-value applications.

We hypothesize that AL can establish electrostatic interactions with Gel and allow the development of Gel-based hydrogels with unprecedented reported mechanical properties, stretchability, and processability. In this work, we describe a class of highly elastic gelatin-alkali lignin (GelAL) hydrogels and inks produced in a single step. The hydrogel's mechanical properties and degradation kinetics can be easily tuned through simple modifications of its composition and/or processing. A colloidal titration and quartz-crystal microbalance with energy dissipation were carried out to further investigate the GelAL materials' interactions. Different post-production processes of the developed GelAL hydrogels can lead to variable degradation times that go from a few hours up to being practically unchanged after 3 months, under physiological conditions. The advanced GelAL hydrogels, designed for stretchability and degradability, exhibited significant promise across a spectrum of biomedical applications, with a particular emphasis on their potential as sustainable hydrogels and inks for 3D printing and scaffolding.

2. Methods

2.1. Materials

AL with low sulfate content; Gel from porcine skin, in powder form, gel strength ~300 g Bloom, type A; and Phosphate buffered saline (PBS) were purchased from Sigma (Saint-Louis, MO, USA). Epichlorohydrin (ECH) was purchased from Laborspirit (Loures, Portugal) and used without further purification.

2.2. Gelatin-alkali lignin (GelAL) hydrogel preparation

The GelAL hydrogels were prepared by dissolving the Gel into a homogeneous AL solution at 70 °C. First, AL was dissolved in deionized water at a final concentration of 5–20% (w/v). The mixtures were placed in a 70 °C water bath and stirred at 300 rpm using a magnetic stirrer. After 1 hour of stirring, Gel powder was mixed into the solution at a final concentration between 10% and 20% (w/v). The mixture was then stirred for a maximum of 15 minutes until complete dissolution of Gel. The resulting hydrogel was then transferred to the desired vessel and let cool down. Hydrogels crosslinked with ECH were cooled down at −20 °C for 20 minutes before being immersed in a solution made of 5% (v/v) of ECH and 95% (v/v) of deionized water, at 20 °C or 37 °C for varying lengths of time. Freeze-dried samples were also produced from the same hydrogels after freezing at −80 °C overnight and drying under vacuum for 24 hours. The hydrogels were then stored at 4 °C before being assessed unless stated otherwise. Herein, 4 different formulations have been produced (Gel10AL5, Gel20AL5, Gel10AL10, and Gel20AL10), which are designated by Gel*x*AL*y* where, *x* and *y* represent the content of Gel and AL in % (w/v), respectively.

2.3. Rheological measurement

The rheological properties of the prepared hydrogels were analyzed using a Kinexus Pro+ rheometer (Malvern Instruments, Malvern, UK) and the rSpace acquisition software (Malvern Instruments, Malvern, UK). Viscometry experiments were performed using a conical stainless steel upper geometry (40 mm diameter, 40° angle) while oscillatory experiments and temperature ramps were performed using a flat stainless steel upper geometry (20 mm diameter). Experiments were performed at 20 °C and 37 °C, and all plots were obtained by averaging at least three samples. The formulations evaluated were Gel10AL5 and Gel20AL10.

2.4. 3D printing process

The printing process was performed on a 3D Bioplotter (4th Generation EnvisionTEC, Gladbeck, Germany). Printed structures were designed with 3D computer-aided design (CAD) modeling using the software Bioplotter RP (EnvisionTEC, Gladbeck, Germany). The created CAD models were converted to an STL motion program, which was read by the bioplotter's control software (VisualMachines, EnvisionTEC, Gladbeck, Germany) to produce physical 3D constructs by ensuring that the material parameters such as printing speed, printing temperature, printing pressure, and substrate temperature were respected during printing.

Printing tests were conducted with the Gel10AL5 ink. A 20 G nozzle (580 μm of diameter, Nordson EFD, Westlake, Ohio, USA) was used to print 3D constructs at 32 °C, with a printing speed of 28 mm/s and an air pressure of 1.2 bar. After printing, the constructs were crosslinked using the same solution made from 5% (v/v) of ECH and 95% (v/v) of deionized water, at room temperature overnight, before being washed 3 times with distilled water.

2.5. Mechanical assessment

Cyclic uniaxial compression of molded cylinders (d=8 mm, h=10 mm) was performed on 6 samples of Gel10AL5 Gel20AL5, Gel10AL10, and Gel20AL10 hydrogels at room temperature, using a Universal Testing Machine (Instron, model5540, Norwood, MA, USA) with a 50 N cell. The crosshead speed was set at 50 mm/min, and cyclic deformation between 60% and 10% of the initial length of the samples was performed 10 times. From the stress−strain curve, the Young's modulus was calculated, as well as the force at 60% deformation for the 1st and 10th compression. The dimensions of each cylinder were measured before and after each test.

Uniaxial compressive tests were performed on molded cylinders (d=8 mm, h=10 mm) of Gel20AL10 after ECH-crosslinking, freeze-drying, and PBS degradation. After production, molded cylinders were immersed in a solution made of 5% (v/v) of ECH and 95% (v/v) of deionized water, at room temperature overnight before being washed 3 times with distilled water, and finally freeze-dried. Then, cylinders were soaked in PBS and left at 37 °C for 1, 7, 14, and 90 days in static conditions before being mechanically characterized. Young's modulus, compressive stress at yield and at maximum force, maximum force, as well as compressive strain at maximum force were measured to determine the impact of residence time over the properties of the hydrogels. Tests were made with 6–10 cylinders on each day.

Tensile testing of 1 mm-thick membranes was performed on the same uniaxial testing machine with a 50 N cell at room temperature. Test membranes were produced by casting: the different hydrogel formulations were produced as previously described but were poured onto a sheet of glass instead. A second sheet of glass was layered on top of the hydrogel, then both sheets were compressed together until a 1 mm gap was achieved. The molds were then stored at −20 °C for 20 minutes for easier removal of the membranes, after which they were stored at 4 °C for 24 hours until being assessed. The test samples were then cut with the required dimensions (w=10 mm, l=25 mm, t=1 mm). No post-processing of the membranes was performed. Two types of tensile tests were then performed. First, a classic tensile test until the break was performed on at least 8 test samples from each formulation. The elongation at break, tensile stress at break, and Young's modulus were all measured. Then a 10-cycle tensile test between 0% and 300% elongation was performed on at least 5 test samples of all formulations. The force, tensile stress, and Young's modulus at 300% elongation were measured, as well as the difference in the force measured at 300% elongation between the 1st and 10th cycle. The crosshead speed was set at 50 mm/min for both tests.

2.6. Micro-computed tomography (micro-CT) characterization

The micro-CT characterization of the Gel20AL10 dry samples (n=3) was done with the SkyScan 1272 micro-CT system (Bruker Micro-CT, Belgium) [31,32]. The samples were scanned at a pixel size of 5 μm and a rotation step of 0.4° using the source voltage of 35 kV and current of 181 μA [33]. The reconstruction of projections and microstructural analysis was done using the software from Bruker.

2.7. Dynamical mechanical analysis (DMA)

DMA measurements of the Gel20AL10 hydrogel samples (n=6) were performed using DMA 8000 equipment (PerkinElmer, USA) in unconfined compression mode. The DMA spectra were obtained between 0.1 Hz and 10 Hz under a fixed strain at 37 °C in a PBS bath [34].

2.8. Degradation assay

The degradation kinetics of the Gel20AL10 formulation in physiologically relevant conditions was evaluated after immersion of the different molded structures in PBS at 37 °C for up to 30 days (0, 3, 7, 14, and 30 days) in dynamic conditions (60 rpm). There were 3 groups of hydrogels: (i) crosslinked at 37 °C for 4 hours in 5% (v/v) ECH solution, (ii) crosslinked at 37 °C for 4 hours in 5% (v/v) ECH solution and freeze-dried, and (iii) crosslinked at 20 °C overnight in 5% (v/v) ECH solution and freeze-dried. For each time point, 6 samples were used from each of the 3 groups, making a total of 30 samples. The samples were weighted before immersion (m_i), after each test period once rinsed with distilled water and dried on a filter paper (m_w), and after freeze-drying (m_d). These measures allowed the calculation of the weight loss (Eq. 1) and water uptake (Eq. 2) of the samples using the following equations:

$$\text{Weight loss } (\%) = (m_i - m_d)/m_i \text{ x } 100\% \quad (1)$$

$$\text{Water uptake } (\%) = (m_w - m_d)/m_d * 100 \quad (2)$$

To measure the ionic strength of the materials, the weight loss and water uptake of the Gel20AL10 formulation were recorded in the same way as previously described. The evaluation was performed after a 72-hour immersion of non-modified samples in solutions of NaCl at different concentrations (0, 0.001 M, 0.01 M, 0.1 M, and 0.5 M) at 37 °C in dynamic conditions (60 rpm) (n≥4).

2.9. Zeta potential measurement

The zeta potential of a 0.1% (w/v) AL solution was measured using a Nano ZS Zetasizer (Malvern Instruments, Malvern, UK) using DTS software (Malvern Panalytical, Malvern, UK). Measurements were performed at 25 °C and the surface charge was calculated using the Smoluchowski model with an F(Ka) value of 1.50. First, the zeta potential of a solution of AL at 0.01% (w/v) and a solution of Gel at 0.5% (w/v) were measured. Then, a colloidal titration was performed using solutions comprising 0.01% (w/v) of AL with various amounts of Gel (0.005, 0.001, 0.05, 0.06, 0.07, 0.08, 0.09, 0.1% (w/v)). The zeta potential of each solution was measured 5 times and each measurement was performed after a 2-minutes stabilization period.

2.10. Quartz crystal microbalance with energy dissipation

A Quartz Crystal Microbalance (Q-Sense E4, QSENCE) was used to characterize the nature of the interaction between the Gel and AL. Crystals were first coated with a solution of 1% (w/v) of polyethylenimine (PEI) before being alternatively coated with a Gel solution at 0.4% (w/v) and a solution of AL at 0.2% (w/v). The flow rate was adjusted to 50 μL/minute and crystals were washed with Milli-Q water between each coating. Solutions were switched after stability was observed in the measured thickness of the coating.

2.11. Statistical Analysis

All the numerical results are presented as mean ± standard deviation (SD). Statistical analysis was performed using GraphPad Prism 9.3 (GraphPad Software, La Jolla, CA, USA). First, a Shapiro-Wilk test was used to ascertain data normality. The differences between the experimental results were analyzed using a one-way ANOVA test followed by Tukey's multiple comparison test, with a single pool variance. The significance levels were set to: *$p < 0.05$, **$p < 0.01$, ***$p < 0.001$.

3. Results and discussion

3.1. Preparation and characterization of the hydrogels

The current global trend of biomedical research leans towards the use of cell-based 3D bioprinting to create 3D functional living tissues, capable of mimicking the complex extracellular matrix (ECM) of native tissues and organs for their future transplantation into patients' bodies [3]. However, the materials currently used in 3D bioprinting have to tradeoff between their mechanical and biological properties. The

general view regarding natural biomaterials is that they often exhibit remarkable biological properties but tend to have limited mechanical strength. Conversely, synthetic biomaterials are known for their impressive mechanical properties but often lack desirable biological characteristics. This simple view lays the basis for the current research in biomaterial science. Extensive modifications of biomaterials can partially solve this trade-off, but often raise other concerns: chemical crosslinking for example, is an efficient and popular way to improve natural polymers' mechanical properties, but densely crosslinked hydrogels have poor cell culture performances because of their limited porosity and permeability, which reduce nutrient diffusion, cell spreading, and migration. Non-modified hydrogels also rarely present elastic and/or self-healing properties. Therefore, practical methods to recreate the native ECM with little chemical modification of biomaterials are needed.

Recently, our team used a bioink of methacrylated silk fibroin along with a bioink of gellan-gum and fibrinogen in a hybrid bioprinting process to produce highly elastic scaffolds which could recover from a 60% compression [35]. Herein, we describe a novel type of hydrogel by means of blending Gel and AL (Table 1). The Gel is a well-known and extensively used biomaterial, which generally needs supplementation for tissue engineering purposes because of its poor mechanical properties. AL, on the other hand, is an underutilized biomaterial that has recently begun to be used to complement other biomaterials for biomedical applications. The described hydrogels were prepared with concentrations of AL varying between 5% and 10% (w/v). The hydrogels were produced in a single-step process in a range of formulations that can recover from repeated deformations up to 80% compression and 300% elongation, and also can be 3D printed (Fig. 1).

3.2. Physico-chemical properties of the hydrogels

The 3D printability of a bioink is strongly affected by the rheological and physicochemical properties of the bioink that define the ability of the bioink to flow through the 3D printer nozzle at a certain rate, keep structural integrity and support cell viability [36–38]. In 3D bioprinting, it is required to find the harmony between mechanical and biological performance. Viscosity and shear thinning characteristics are among the rheological properties of bioinks. Bioinks require high viscosities to achieve high resolutions by reducing material spreading and deformation upon deposition. However, high-viscosity bioinks induce a lot of shear stresses on suspended cells during printing, which has a direct negative impact on cell viability. A bioink with shear-thinning behavior has a decreasing shear viscosity with the shear rate increasing. Such types of bioinks will therefore act as solid at rest, as liquid when shear is applied, and reform to a solid after shear stress is removed. This property allows a reduction in cell shear stress during extrusion and reduces material deformation after deposition. For bioinks, lower concentrations are preferred since they require lower extruding pressure, resulting in lower shear stresses applied to the encapsulated cells [39]. Higher concentrations of AL can be used for molded applications and are associated with higher mechanical strengths and longer residence times. AL concentrations lower than 5% (w/v) display poor elasticity, while concentrations higher than 10% (w/v) are too viscous and difficult to work with. Similarly, the Gel content of the hydrogels varies between 10% and 20% (w/v). The concentration of Gel is defined by the intended purpose and/or desired features. Once again, lower concentrations are generally preferred for 3D extrusion (bio)printing purposes as they have been found to require lower extruding pressure and/or extruding temperatures. Higher concentrations of Gel can be used for applications that require superior mechanical strength or degradation times. For formulations with concentrations lower than 10% (w/v) gelation does not occur at room temperature, whereas those with concentrations higher than 20% (w/v) are prone to create bubbles that are difficult to remove, making processing difficult. Stirring should ideally not be done for longer than 15 minutes after which, the mixture tends to become highly viscous, difficult to work with, and prone to form bubbles. After stirring and complete dissolution, the reaction mixture is left to cool down in the appropriate vessel. For 3D printing applications, the mixture can be directly loaded into a printer cartridge and stored at 4 °C. It can also be cast into the desired mold to produce hydrogels or membranes. It is well known that Gel is a temperature-sensitive material. Therefore, it is expected that the developed hydrogels and inks to present different mechanical properties when processed at different temperatures.

Table 1
Hydrogel formulations.

Hydrogel designation	Content of Gel [%(w/v)]	Content of AL [%(w/v)]
Gel10AL5	10	5
Gel20AL5	20	5
Gel10AL10	10	10
Gel20AL10	20	10

In this study, the hydrogels developed showed a shear-thinning behavior at different temperatures which can be correlated with their compositions. These properties can be attributed to lignin which is a shear-thinning polymer whereas Gel displays a reversible gelation mechanism upon heating. This shear-thinning behavior is followed by a crosslinking mechanism and an increase in viscosity at higher temperatures which depend on the lignin source and extraction method. Given that hydrogels composed only of Gel do not present such rheological behavior without chemical processing, it is believed that the dynamic interactions such as electrostatic interactions or hydrogen bonding between Gel and AL are at the origin of this shear-thinning behavior. Fig. 2 presents the rheological (Fig. 2a) and mechanical properties (Fig. 2b-c) of the hydrogels. It was observed that although the decrease in shear viscosity is observed at a similar shear rate, there is a 2- to 7-fold increase between the shear viscosity values of the Gel10AL5 and the Gel20AL10 hydrogels.

The Gel10AL5 hydrogels were found to be better suited for 3D (bio) printing applications, and it is possible to achieve different internal architectures via different directions of strands among the layers. It was observed that the 3D-printed structure was fragile immediately after printing, but could be easily manipulated after crosslinking and even after having spent 7 days in physiological conditions. Once crosslinked, the structure could be stretched and deformed without breaking, even after 7 days of degradation in physiological conditions. Moreover, printed structures were sticky and could attach to any surface they touched immediately after the printing process, whereas after crosslinking they lost this property.

Mechanical and micro-structural properties are fundamental aspects of biomedical devices as the successful integration of implanted structures in patients' bodies relies on their ability to mimic natural tissues, especially for cell-laden hydrogels as it is well known that cell differentiation is influenced by their substrates' structure and mechanical properties [40–42]. Native tissues cover a large range of mechanical properties [43,44]. Therefore, it is important to be able to tune the properties of implanted scaffolds to closely mimic those of the tissues they aim to replace/regenerate. To determine the impact of the content of Gel and AL on the mechanical properties of the hydrogels, samples were subjected to cyclic compressive, tensile, and cyclic tensile tests. First, cylindrical samples (d=8 mm, h=10 mm) of Gel10AL5, Gel20AL5, Gel10AL10, and Gel20AL10 were tested on a uniaxial compression equipment during cyclic compression tests. The maximum force and Young's moduli of the hydrogels were measured during the first compression, as well as the difference in the maximum force between the 1st and 10th compression and the height loss induced by the test, were investigated (Fig. 2b). These tests indicate that the values of the hydrogels' Young's moduli (0.42 ± 0.09–0.93 ± 0.14 MPa) are comparable to that found for soft tissues such as the skin, bladder, cornea, and gut [45]. These tests also demonstrate that the content of Gel has a

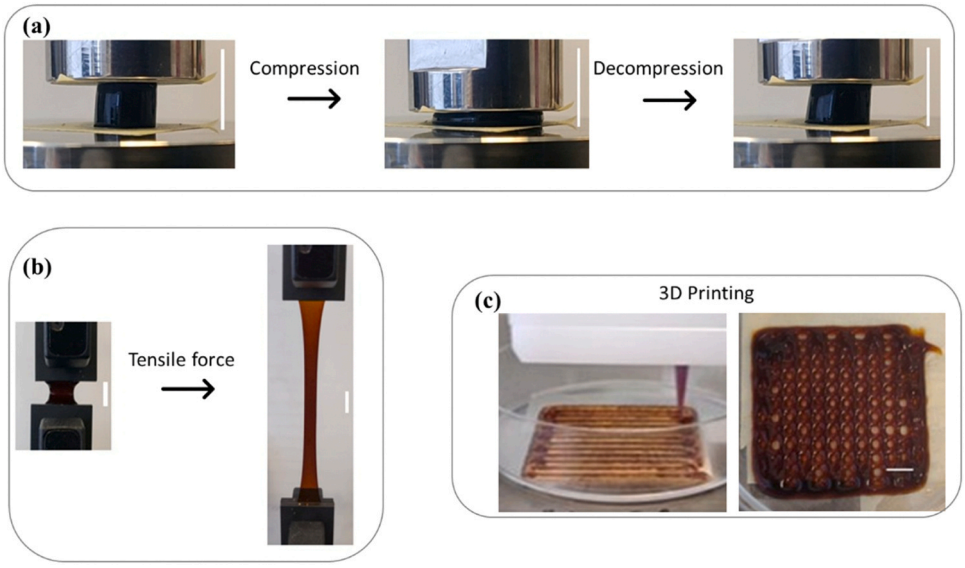

Fig. 1. a) Compression cycle (up to 80% strain) of a cylinder-shaped Gel10AL5 hydrogel, b) tensile testing at 700% of a cast membrane of Gel20AL10 hydrogel, c) 3D-printing process using the Gel10AL5 ink (left), and an example of a 3D-printed hydrogel. The scale bars indicate 10 mm in a and b, and 500 μm in c.

significant impact on the mechanical properties of the hydrogels: formulations with a double content of Gel present more than double the force at 60% strain (from 3.37 ± 0.46 MPa up to 6.73 ± 0.9 MPa for formulations with 5% (w/v) AL and from 2.91 ± 0.44 MPa up to 7.17 ± 1.35 MPa for those containing 10% (w/v) AL). Higher contents of Gel also seem to increase the hydrogels' recovery as the difference in the maximum force measured during the 1st and 10th compression is more 50% lower for formulations with twice the Gel contents (from 17.11 ± 4.77% up to 7.98 ± 1.7% for formulations with 5% (w/v) AL and from 21.18 ± 5.12% to 9.79 ± 3.35% for those containing 10% (w/v) AL). Finally, the formulations with higher Gel content also generally display less height loss induced by repeated compression, but with no statistically significant difference. However, this height loss was only temporary as the test samples recovered their normal height within 5 minutes after the loads were removed. This was also observed for a cyclic test at 80% for the Gel10AL5 hydrogel. Only this formulation has been evaluated at 80% strain as other formulations would require forces that were above 50 N and, therefore, outside the limits of our uniaxial testing machine. The stress-strain curves of the hydrogels obtained by the tensile and compression tests are presented in supplementary material (Figure S1).

The tensile properties of all formulations using tensile testing were also characterized. The elongation at break, tensile stress at break, and Young's modulus recorded are displayed in Fig. 2c. Both the content of Gel and AL impact the properties of the hydrogels, but the impact induced by the content of AL was only significant for the formulations with 20% (w/v) Gel. The tensile stress at the break for the Gel20AL10 formulation was 0.62 ± 0.1 MPa, which is 63% higher than that of Gel20AL5 (0.38 ± 0.07 MPa) and 250% higher than that of Gel10AL10 (0.18 ± 0.04 MPa). The differences were lower for the Young's modulus as the value measured for the Gel20AL10 formulation was 0.14 ± 0.02 MPa, 32% higher than the value for Gel20AL5 (0.1 ± 0.03 MPa) and 157% higher than that of Gel10AL10 (0.05 ± 0.01 MPa). The elongation at break also decreased as it averaged 659 ± 149% for the Gel20AL10 formulation, which is 20% more than that of Gel20AL5 (547 ± 97%) and 55% more than the average elongation at break of Gel10AL10 (425 ± 101%). In brief, these stretchable and tough hydrogels revealed unique features and tunability that deserve further exploitation in mechanical sensing or even in drug delivery, in future studies.

Fig. 3 presents the micro-structural properties (Fig. 3a) and the dynamic mechanical properties (Fig. 3b) of Gel20AL10 hydrogels. The micro-CT analysis (Fig. 3a) of Gel20AL10 hydrogels showed that the mean porosity of the samples was 64.5 ± 7.1%, the mean wall thickness and mean pore size was 38.3 ±3.3 μm and 310.1 ± 141.4 μm, respectively. Around half of the pores were in the range between 5 and 205 μm. Based on the DMA results (Fig. 3b), the storage modulus (E') indicated the sample stiffness and was found to be in the range between 0.055 and 0.061 MPa, loss factor (tan δ) indicates the damping properties and is in the range between 0.09 and 0.12, and loss modulus (E'') indicates the energy dissipation and found to be the range of 0.005–0.007 MPa. Overall, the DMA results showed the viscoelastic characteristics of the hydrogels.

Cyclic tensile testing was also performed on the developed formulations. Test samples were produced for normal tensile testing and were then stretched at 300% elongation 10 times. The maximum force, tensile stress at maximum elongation, Young's modulus, and the elongation induced by the cyclic test are displayed below (Fig. 4a). Similarly, the content of Gel and AL impacted the properties of the hydrogels, but significant differences induced by the content of AL were mostly observed in formulations containing 20% (w/v) of Gel only. For the maximum force for example, the difference measure between the values of Gel10AL5 and Gel20AL5 was only 43% (from 0.94 ± 0.14 MPa to 1.34 ± 0.21 MPa) whereas the difference was 96% between Gel10AL10 and Gel20AL10 (from 1.13 ± 0.29 MPa to 2.22 ± 0.32 MPa). This trend was also observed for the tensile stress and the Young's modulus. However, hydrogels with higher contents of Gel did not recover well from cyclic tensile tests as they would often break during repeated elongations at 300%, and these formulations remained more elongated after the cyclic stretching than formulations with 10% (w/v) Gel. Moreover, the edges of these hydrogels would dry up during cyclic elongations, which was irreversible. The weight loss and water uptake profile of the Gel20AL10 hydrogel formulations with different post-production processes were evaluated. Fig. 4b presents the corresponding data in PBS, and NaCl solutions, Fig. 4c shows the mechanical properties upon degradation as discussed below. The non-modified hydrogels are degraded within 12 hours of soaking which is too short for tissue engineering but can be utilized in drug and cell delivery applications. Different crosslinking temperatures and crosslinking times were studied, and it was observed that heating up the hydrogels at 37 °C during the crosslinking process would induce partial melting, resulting in the deformation of the hydrogels. Therefore, crosslinking

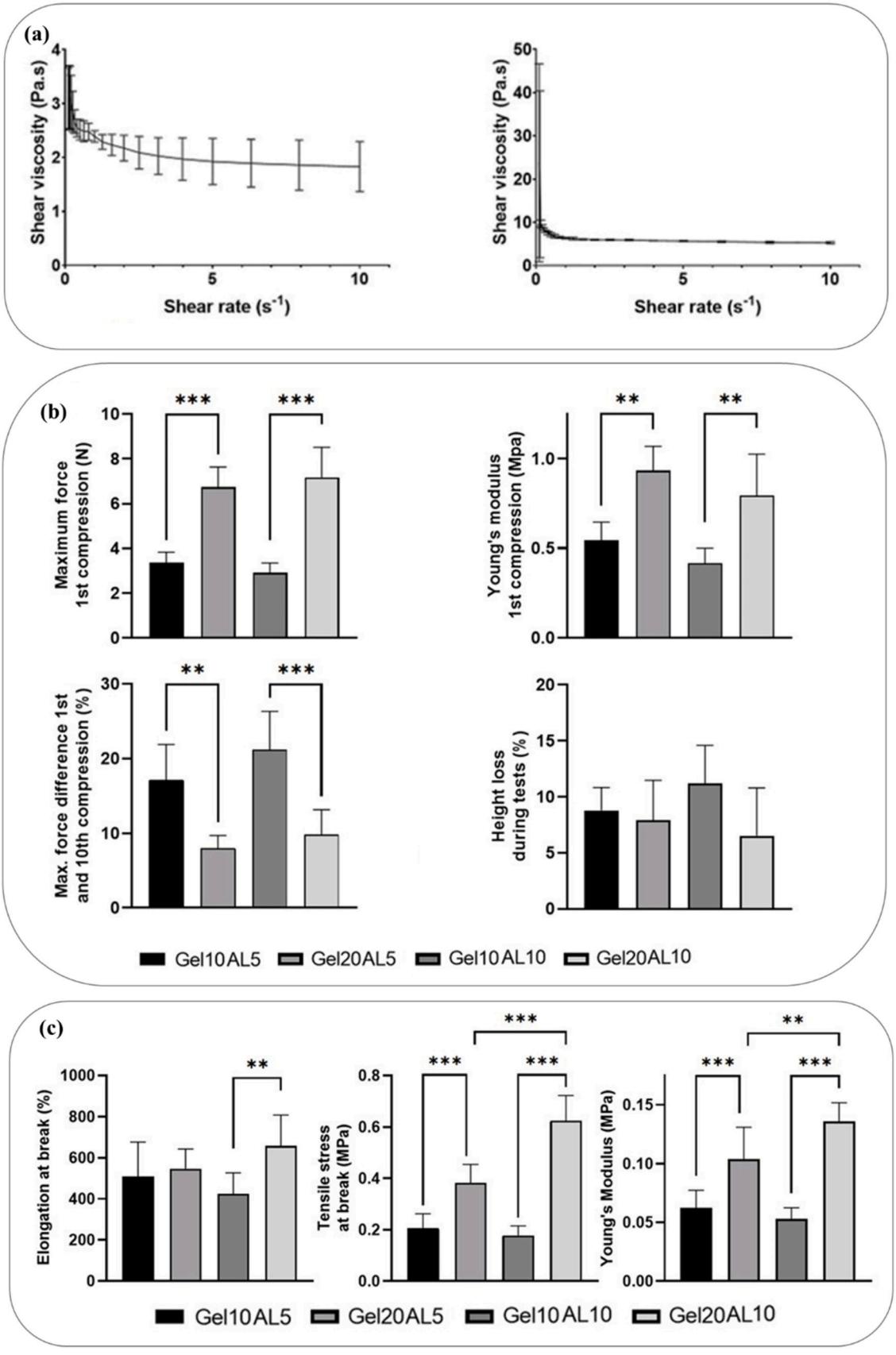

Fig. 2. a) The shear viscosity as a function of shear rate for Gel10AL5 hydrogel at 32 °C (left) and for Gel20AL10 hydrogel at 37 °C (right), b) The maximum force and Young's modulus measured during the first compression (top), the difference in the maximum force between the 1st and 10th compression, and the height loss induced by 10-cycle compression tests between 10% and 60% strain (bottom), depending on the composition of the hydrogels, and c) the elongation, tensile stress at break, and Young's modulus depending on the composition of the hydrogels. The significance level was set to: *$p < 0.05$, **$p < 0.01$, ***$p < 0.001$.

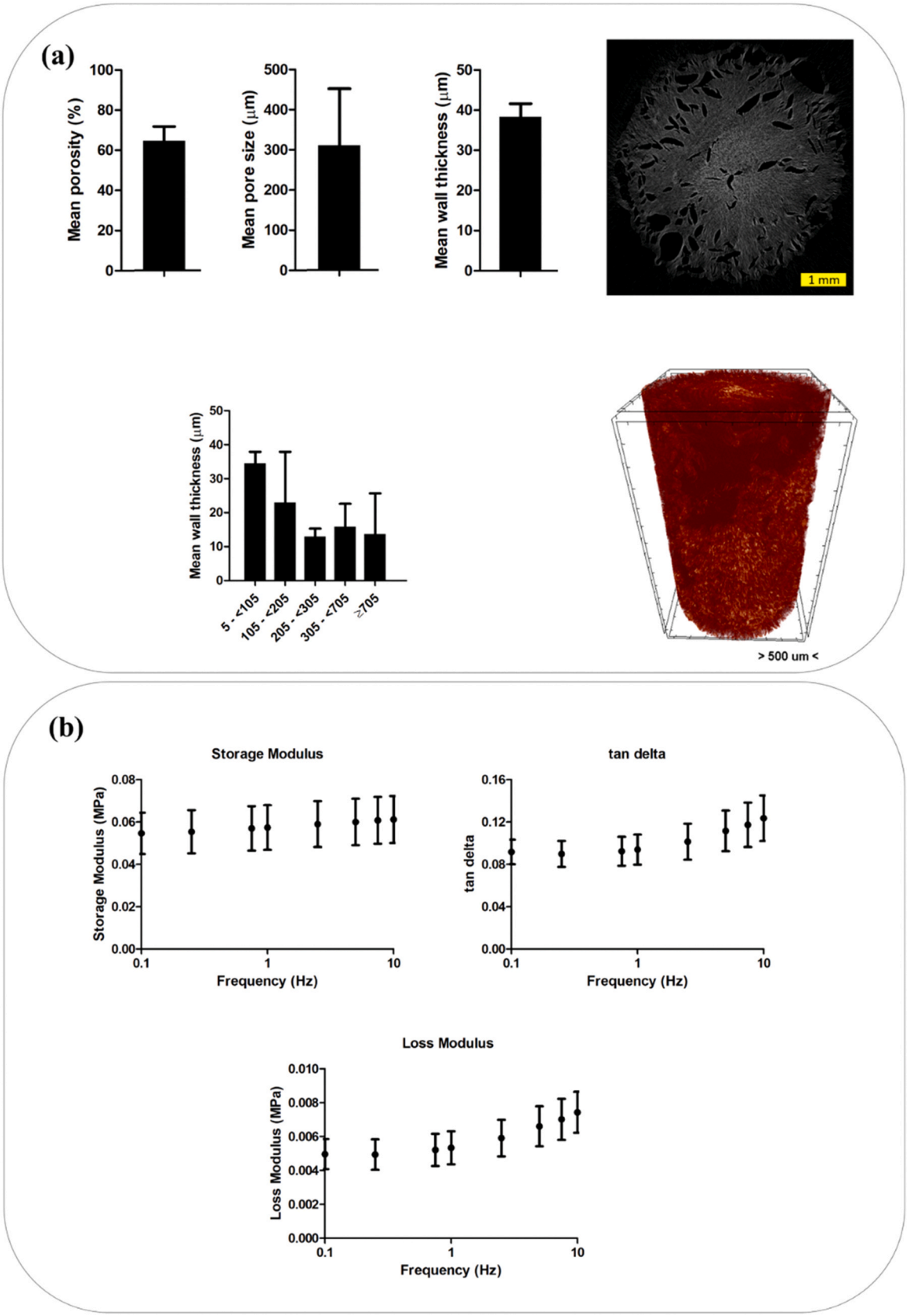

Fig. 3. a) Micro-CT results of Gel20AL10 hydrogels indicating the micro-structural characteristics of the samples: mean porosity, mean wall thickness, and mean pore size (top left), pore size distribution (bottom left), a 2D cross-sectional image, the scale bar indicates 1 mm, (top right), a 3D reconstructed image of the sample, the scale bar indicates 500 μm that is the length between the ticks (bottom right), and b) DMA results of Gel20AL10 hydrogels indicating the storage modulus, loss modulus, and tan δ values.

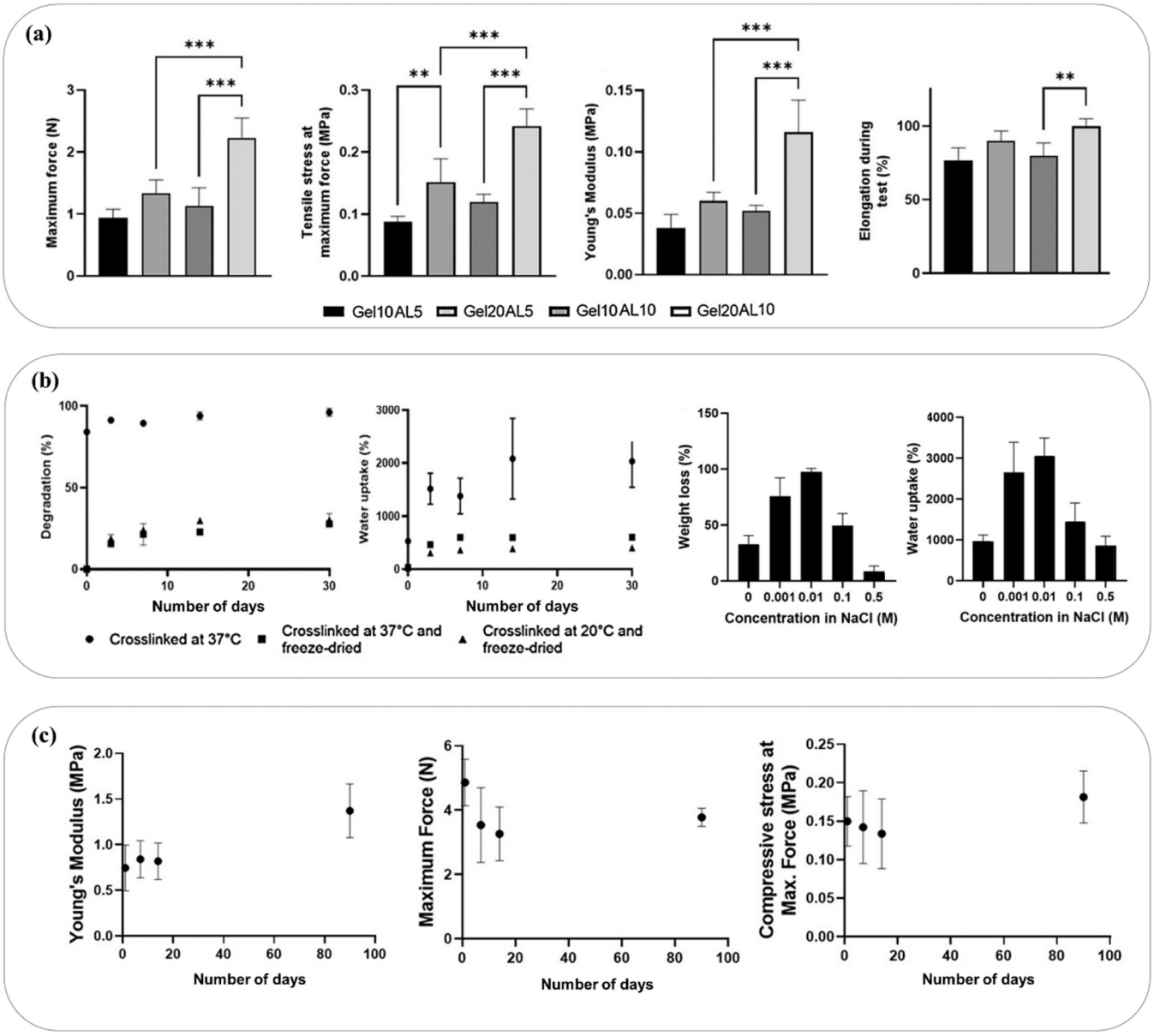

Fig. 4. a) The maximum force, tensile stress at maximum elongation, Young's modulus, and elongation of the samples after 10-cycle tensile tests between 0% and 300% elongation depending on the composition of the hydrogels. The significance level was set to: *$p < 0.05$, **$p < 0.01$, ***$p < 0.001$. b) Degradation and water uptake profiles of Gel20AL10 hydrogels in PBS, and NaCl solutions after 72 hours of soaking, and c) the Young's modulus, maximum force, and compressive stress at maximum force of Gel20AL10 hydrogels that were crosslinked at room temperature overnight.

protocols at lower temperatures and longer times were evaluated, namely overnight crosslinking at room temperature, and 2-day crosslinking at 4 °C. The latter method did not induce crosslinking of the material, even at higher ECH concentrations, and test samples completely dissolved within 12 hours of soaking similarly to non-crosslinked samples, while crosslinking at room temperature overnight proved to be highly effective. Although it is generally recommended to use elevated crosslinking temperature with lignin, this study showed that lower temperatures associated with longer crosslinking times are an effective alternative.

The hydrogels that had been crosslinked at room temperature overnight and then freeze-dried showed slower degradation and water uptake. Freeze-drying was also shown to greatly enhance their residence times. The samples displayed different degradation profiles depending on their post-production processes. The hydrogels crosslinked at 37 °C that were not freeze-dried underwent rapid water uptake during the first 3 days (from 527.86% ± 25.21% on day 0–1514.82% ± 282.17% on day 3, or a 287% increase). Water uptake then stabilized at around 2000% around day 14. By its turn, the hydrogels crosslinked and freeze-dried underwent a slower water uptake. Those which had been crosslinked at 37 °C reached 600% water uptake on day 7 and remained stable until day 30, while the samples which had been crosslinked at 20 °C saw their water uptake continuously increasing during the 30 days of soaking until reaching 399.02% ± 56.20%.

This work showed that these hydrogels possess highly tunable degradation profiles. However, these modifications come at a cost: ECH is a toxic chemical that must be washed off, and freeze-drying impacts the appearance of hydrogels and mechanical properties by shrinking and making them stiff and brittle. Re-hydration of freeze-dried samples allowed the hydrogels to retrieve their softer mechanical properties. Future studies should finely tune the crosslinking parameters to achieve successful crosslinking and degradation tunability with no shape change, and future cellular studies should include washing steps for the hydrogels to thoroughly remove ECH before cells are seeded, which can

be done during re-hydration after freeze-drying. Overall, the degradability results demonstrated that GelAL hydrogels/inks can be tuned to fit different applications and the potential application of these hydrogels as wearable sensors [46] can be envisioned, as materials should generally be highly stretchable to provide comfort for the wearer.

The weight loss and water uptake of the Gel20AL10 formulation were recorded after immersion of the samples in NaCl solutions for 72 hours (Fig. 4b) to determine the impact of the ionic strength of the environment on their degradation kinetics. The samples immersed in higher concentrations of NaCl experienced less weight loss and water uptake as compared to the other samples. The Gel is not known to experience ionic crosslinking, contrarily to lignin which can experience hydrogen bonds, covalent, and π - π stacking interactions as highlighted by previous works [47]. However, a great disparity of the results was observed for samples immersed in distilled water (the weight loss averaged 53.69 ± 33.49% and the water uptake averaged 1895 ± 1456%).

When hydrogels are investigated for their potential use in biomedical and tissue engineering applications, the hydrogel's stability/degradability over time is a critical factor that needs to be known. Thus, the

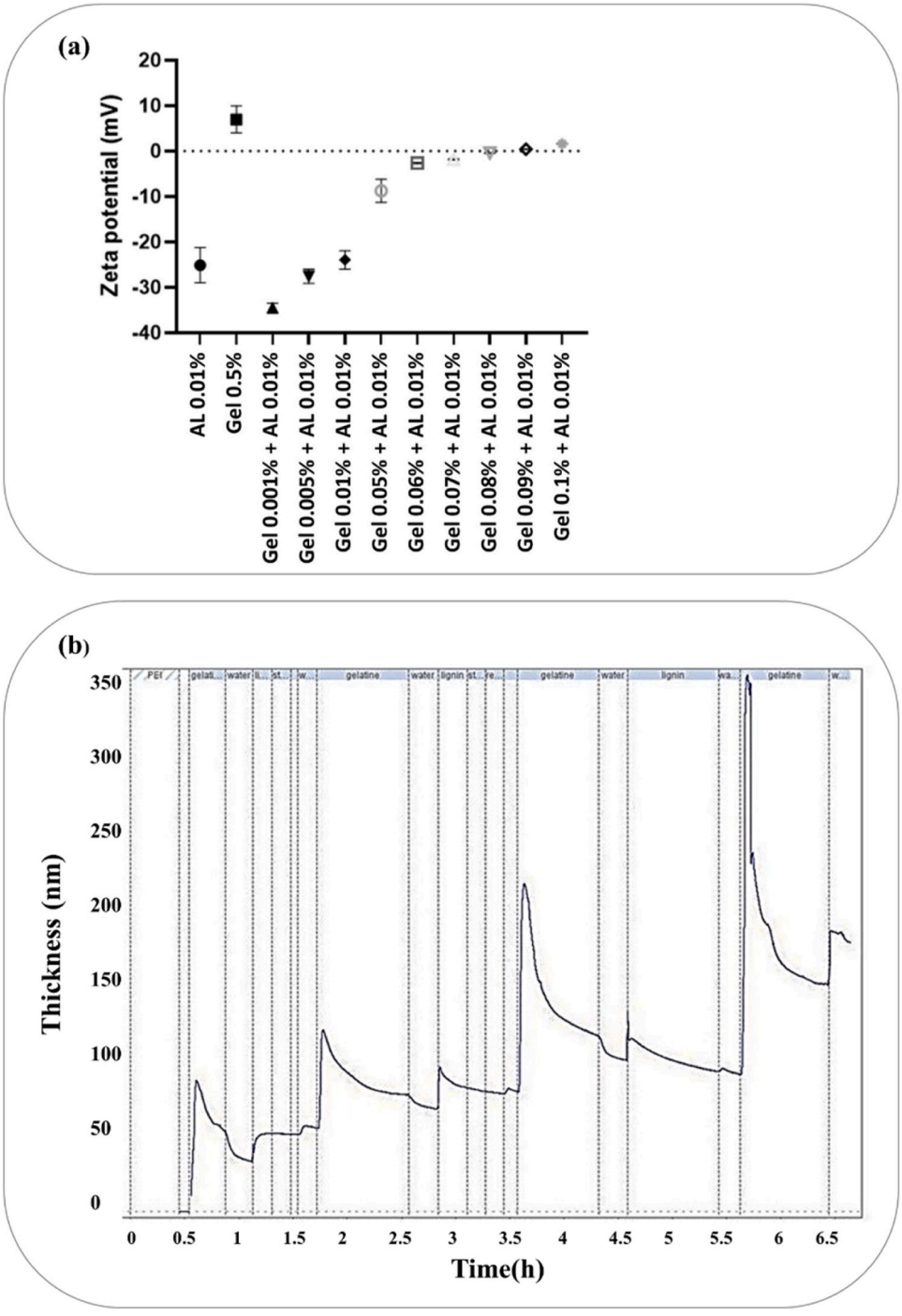

Fig. 5. a) Colloidal titration of a solution of AL at 0.01% with increasing concentrations of Gel. The AL has a negative zeta potential while the Gel has a positive one. The addition of Gel into the AL creates electronically neutral complexes which bring the overall zeta potential of the solutions closer to 0, and according to this experiment, a GelAL solution at an 8:1 mass ratio has a neutral zeta potential, and b) Quartz Crystal Microbalance assay indicating the thickness of material deposited on the sensor during QCM-D assessment is then recorded in real-time.

mechanical characterization of Gel20AL10 hydrogels which had been previously crosslinked with ECH and freeze-dried, and the evolution of their mechanical properties over time (1, 7, 14, and 90 days) in PBS at 37 °C and static conditions were also assessed. The samples were tested in uniaxial compression and their Young's modulus, compressive stress at yield, maximum force, compressive stress, and strain at maximum force were measured. Over the course of the 90-day degradation in physiological conditions, the mechanical properties of the samples were shown to vary. As seen in Fig. 4c, the hydrogels become softer during the first two weeks, before becoming stiffer over time as the maximum force measured during compression would go from 4.86 ± 0.73 N on day 1–3.26 ± 0.84 N on day 14, and then to 3.78 ± 0.28 N on day 90. A similar trend was also observed for the compressive stress. However, the hydrogels would also generally become more brittle over time as the compression strain at maximum force continuously decreased from 27.95 ± 10.06% on day 1–15.79 ± 12% on day 90, while the Young's modulus increased from 0.75 ± 0.25 MPa on day 1–1.37 ± 0.3 MPa on day 90. The compressive stress at maximum force and the maximum force both decreased for the first 2 weeks before increasing back up, indicating a softening phase followed by a hardening phase. This softening phase could be explained by a progressive fluid uptake from the hydrogels.

3.3. Interactions between Gel and AL

In addition to mechanical tests, zeta potential measurements, a colloidal titration, and quartz crystal microbalance with energy dissipation tests were performed to unveil the nature of the interactions between Gel and AL. The increase of tensile properties with a higher content of both Gel and AL might be due to their interaction. Lignin presents anionic sulfonates which could interact with the arginine and lysine residues from Gel, to create reversible and dynamic interactions. The selected lignin has a low concentration of sulfonates, which have been demonstrated by various studies to present cytotoxicity. Nonetheless, despite the low concentration of sulfonates, an AL solution at a concentration of 0.01% (w/v) displayed a zeta potential equal to −25.1 mV, while a solution of 0.5% (w/v) of Gel presented a zeta potential equal to 6.994 mV. The colloidal titration proved that adding Gel to an AL solution would shift its zeta potential towards positive values. Fig. 5a shows that the shift between negative and positive values would occur at a weight ratio of 1:8.5 between AL and Gel. Overall, this assay demonstrated that Gel and AL would form neutral complexes when mixed. In addition to the zeta potential measurements, a quartz crystal microbalance with energy dissipation was used to further characterize the interactions between AL and Gel (Fig. 5b). This assay revealed that AL and Gel readily bound through weak interactions and alternating flows of AL and Gel gradually coated the sensor. This layer of material is progressively washed off, as depicted by peaks in the curve of the thickness of material deposited on the sensor during the assessment. We first hypothesized that the dynamic nature of this test was the reason behind this washing-off, however, it kept occurring even when the flow was stopped (between 1h15 and 1h25, and between 3h03 and 3h13. These peaks are also correlated with the viscosity of the material being circulated: peaks generated by the introduction of the Gel solution are higher than those induced by the AL solution due to the higher viscosity of the Gel solution. No clear steps being marked by the introduction of the different coatings indicated that the material deposited may have some peculiar conformation, being worth in-depth investigation in future works.

This study has certain limitations and shortcomings as, in 3D-printing, only acellular hydrogels were printed with only basic infill patterns, namely lines with certain angles, and *in vitro* cell culture work with the proposed hydrogels is not a part of the present study. To conclude, the future works include: i) 3D printing of hydrogels with more complex infill patterns and 3D shapes, ii) inclusion of cells for bioprinting, and iii) *in vitro* cell culture studies to evaluate the performance of both cell-seeded hydrogels and cellular hydrogels obtained by 3D printing using the bioink, in cell culture. Being stretchable and tough hydrogels, the analysis of conductivity and pressure sensing characteristics of the proposed GelAL formulations and their change under mechanical stress will be also investigated in order to further unveil their potential for application as flexible sensors.

4. Conclusion

Lignin has recently gained a lot of attention in numerous applications thanks to its high availability and possibility of functionalization. Yet, it remains underutilized due to its highly heterogeneous nature. The highly stretchable and tough gelatin-alkali lignin hydrogels presented herein are an inexpensive, sustainable material that displays mechanical properties that are rarely seen in biomaterials. It can also be easily produced and tuned to fit the requirements of different fields. Along with several other advantageous properties, the gelatin-alkali lignin hydrogels present tailorable mechanical properties and processing temperature according to their formulation, tunable degradation kinetics which can be easily increased by various processes, and can be cast molded for producing scaffolds, and processed as inks for finding applications in 3D printing. Thus, the highly elastic and tough gelatin-alkali lignin materials appear as versatile hydrogel platforms that can potentially suit numerous biomedical and/or industrial applications. Due to their unique stretchability and tunable degradation kinetics, their potential in the field of mechanical sensing (wearables) and drug delivery warrants further exploration in future research works.

CRediT authorship contribution statement

Joana Silva-Correia: Writing – original draft, Supervision, Resources, Funding acquisition. **Joaquim Miguel Oliveira:** Writing – review & editing, Writing – original draft, Supervision, Resources, Funding acquisition. **Maurice N. Collins:** Supervision, Resources, Funding acquisition. **Rui L. Reis:** Supervision, Resources, Funding acquisition. **Ibrahim Fatih Cengiz:** Writing – review & editing, Writing – original draft, Investigation. **João B. Costa:** Investigation. **Guy Decante:** Writing – original draft, Investigation.

Declaration of Competing Interest

The authors declare that they have no known competing financial interests or personal relationships that could have appeared to influence the work reported in this paper.

Data availability

Data will be made available on request.

Acknowledgments

The authors would like to thank the financial support provided through the projects B-Fabulus "Biofabricação de estruturas 3D funcionalizadas para regeneração meniscal personalizada" (PTDC/BBB-ECT/2690/2014), 3BioMeD (JICAM/0001/2017) and B-Liver (PTDC/EMD-EMD/29139/2017), financed by the Portuguese Foundation for Science and Technology (FCT) and COMPETE 2020. Additionally, this study received financial support from the European Commission funded Oncoscreen project (Grant agreement ID: 101097036). The authors also thank to the FEDER program for funds provided under JUSTHera project (NORTE-01-0145-FEDER-000055) and the 0624_2IQBIONEURO_6_E project (Inter-regional cooperation program VA Spain-Portugal POCTEP 2014–2020). The authors also thank the financial support provided under the project "HEALTH-UNORTE: Setting-up biobanks and regenerative medicine strategies to boost research in cardiovascular, musculoskeletal, neurological, oncological, immunological and infectious

diseases", reference NORTE-01–0145-FEDER-000039, funded by the Norte Portugal Regional Coordination and Development Commission (CCDR-N), under the NORTE2020 Program. The authors also thank the "TERM RES Hub – Scientific Infrastructure for Tissue Engineering and Regenerative Medicine", reference PINFRA/22190/2016 (Norte-01–0145-FEDER-022190), funded by the FCT in cooperation with the Northern Portugal Regional Coordination and Development Commission (CCDR-N), for providing relevant lab facilities, state-of-the art equipment, and highly qualified human resources. Authors also thank FCT for the LA ICVS/3B's fundings: i) funding "Base": DOI 10.54499/UIDB/50026/2020 (https://doi.org/10.54499/UIDB/50026/2020); ii) funding "Programático": DOI 10.54499/UIDP/50026/2020 (https://doi.org/10.54499/UIDP/50026/2020), and iii) funding "Complementar - LA": DOI 10.54499/LA/P/0050/2020 (https://doi.org/10.54499/LA/P/0050/2020). IFC acknowledges the FCT distinction attributed to IFC under the Estímulo ao Emprego Científico program (2021.01969.CEECIND) (https://doi.org/10.54499/2021.01969.CEECIND/CP1664/CT0017). JS-C acknowledges the individual contract under the project LA ICVS-3Bs, references UIDB/50026/2020 and UIDP/50026/2020, financed by national funds, through the FCT and, when eligible, co-financed by EU funds.

Appendix A. Supporting information

Supplementary data associated with this article can be found in the online version at doi:10.1016/j.mtcomm.2024.108875.

References

[1] A. Cappitti, F. Palmieri, R. Garella, A. Tani, F. Chellini, M.S. De Luna, C. Parmeggiani, R. Squecco, D. Martella, C. Sassoli, Biomater. Adv. 155 (2023) 213674.
[2] K. Khoshmaram, F. Yazdian, Z. Pazhouhnia, N. Lotfibakhshaiesh, Biomater. Adv. 156 (2024) 213677.
[3] S.V. Murphy, A. Atala, Nat. Biotechnol. 32 (2014) 773–785.
[4] I. Cengiz, M. Pitikakis, L. Cesario, P. Parascandolo, L. Vosilla, G. Viano, J. Oliveira, R. Reis, Bioprinting 1 (2016) 1–10.
[5] I.F. Cengiz, H. Pereira, M. Pitikakis, J. Espregueira-Mendes, J.M. Oliveira, R. L. Reis, Bio Orthop. N. Approach (2017) 411–418.
[6] D. Ciolacu, Sustain. Biomass-.-. Bio-Based Chem. (2021) 161.
[7] G. Marcì, G. Mele, L. Palmisano, P. Pulito, A. Sannino, Green. Chem. 8 (2006) 439–444.
[8] M.K. Azeem, A. Islam, R.U. Khan, A. Rasool, M.A.U.R. Qureshi, M. Rizwan, F. Sher, T. Rasheed, Polym. Adv. Technol. 34 (2023) 3046–3062.
[9] R. Kundu, P. Mahada, B. Chhirang, B. Das, Current research in green and sustainable, Chemistry 5 (2022) 100252.
[10] Z. Zhang, N. Abidi, L. Lucia, S. Chabi, C.T. Denny, P. Parajuli, S.S. Rumi, Carbohydr. Polym. 299 (2023) 120140.
[11] S. Chang, S. Wang, Z. Liu, X. Wang, Gels 8 (2022) 389.
[12] H. Li, Z. Hao, S. Zhang, B. Li, Y. Wang, X. Wu, Y. Hu, R. Chen, T. Chen, J. Li, Macromol. Biosci. (2023) 2200481.
[13] Z. Maan, N.Z. Masri, S.M. Willerth, Biomolecules 12 (2022) 141.
[14] A. Papaioannou, E. Vasilaki, K. Loukelis, D. Papadogianni, M. Chatzinikolaidou, M. Vamvakaki, Biomater. Adv. (2023) 213737.
[15] T. Gupta, S.B. Ghosh, S. Bandyopadhyay-Ghosh, M. Sain, Biofabrication (2023).
[16] S. Raees, F. Ullah, F. Javed, H.M. Akil, M. Jadoon, M. Safdar, I.U. Din, M. A. Alotaibi, A.I. Alharthi, M.A. Bakht, Int. J. Biol. Macromol. (2023) 123476.
[17] B. Lv, L. Lu, L. Hu, P. Cheng, Y. Hu, X. Xie, G. Dai, B. Mi, X. Liu, G. Liu, Theranostics 13 (2023) 2015.
[18] M.G. Raucci, U. D'Amora, A. Ronca, C. Demitri, L. Ambrosio, Front. Bioeng. Biotechnol. 7 (2019) 27.
[19] Y. Mukheja, J. Kaur, K. Pathania, S.P. Sah, D.B. Salunke, A.T. Sangamwar, S. V. Pawar, Int. J. Biol. Macromol. (2023) 124601.
[20] F.G. Calvo-Flores, J.A. Dobado, ChemSusChem 3 (2010) 1227–1235.
[21] J.M. Lang, U.M. Shrestha, M. Dadmun, Front. Energy Res. 6 (2018) 4.
[22] R. Katahira, T.J. Elder, G.T. Beckham, (2018).
[23] M.S. Ganewatta, H.N. Lokupitiya, C. Tang, Polymers 11 (2019) 1176.
[24] X. Liu, F.P. Bouxin, J. Fan, V.L. Budarin, C. Hu, J.H. Clark, ChemSusChem 13 (2020) 4296–4317.
[25] N. Nan, W. Hu, J. Wang, Biomedicines 10 (2022) 747.
[26] J.B. Johnson, D.A. Broszczak, J.S. Mani, J. Anesi, M. Naiker, J. Pharm. Pharmacol. 74 (2022) 485–502.
[27] X. Wang, Y. Liu, Z. Wu, P. Zhang, X. Zhang, Antioxidants 11 (2022) 253.
[28] W.A. Laftah, W.A. Wan Abdul Rahman, J. Nat. Fibers 13 (2016) 85–102.
[29] P. Schlee, O. Hosseinaei, D. Baker, A. Landmér, P. Tomani, M.J. Mostazo-López, D. Cazorla-Amorós, S. Herou, M.-M. Titirici, Carbon 145 (2019) 470–480.
[30] D. Kai, M.J. Tan, P.L. Chee, Y.K. Chua, Y.L. Yap, X.J. Loh, Green. Chem. 18 (2016) 1175–1200.
[31] I.F. Cengiz, F.R. Maia, A. da Silva Morais, J. Silva-Correia, H. Pereira, R.F. Canadas, J. Espregueira-Mendes, I.K. Kwon, R.L. Reis, J.M. Oliveira, Biofabrication 12 (2020) 025028.
[32] I.F. Cengiz, H. Pereira, J. Espregueira-Mendes, I.K. Kwon, R.L. Reis, J.M. Oliveira, J. Mater. Sci. Mater. Med. 30 (2019) 1–17.
[33] I.F. Cengiz, J.M. Oliveira, R.L. Reis, J. Mater. Sci. Mater. Med. 28 (2017) 1–11.
[34] H. Pereira, S. Caridade, A. Frias, J. Silva-Correia, D. Pereira, I. Cengiz, J. Mano, J. M. Oliveira, J. Espregueira-Mendes, R. Reis, Osteoarthr. Cartil. 22 (2014) 1271–1281.
[35] J.B. Costa, J. Park, A.M. Jorgensen, J. Silva-Correia, R.L. Reis, J.M. Oliveira, A. Atala, J.J. Yoo, S.J. Lee, Chem. Mater. 32 (2020) 8733–8746.
[36] S. Chae, D.-W. Cho, Acta Biomater. 156 (2023) 4–20.
[37] Y.-W. Ding, X.-W. Zhang, C.-H. Mi, X.-Y. Qi, J. Zhou, D.-X. Wei, Smart Mater. Med. 4 (2023) 59–68.
[38] S. You, Y. Xiang, H.H. Hwang, D.B. Berry, W. Kiratitanaporn, J. Guan, E. Yao, M. Tang, Z. Zhong, X. Ma, Sci. Adv. 9 (2023) eade7923.
[39] G. Decante, J.B. Costa, J. Silva-Correia, M.N. Collins, R.L. Reis, J.M. Oliveira, Biofabrication 13 (2021) 032001.
[40] C.R. Alcala-Orozco, X. Cui, G.J. Hooper, K.S. Lim, T.B. Woodfield, Acta Biomater. 132 (2021) 188–216.
[41] K. Elkhoury, M. Morsink, L. Sanchez-Gonzalez, C. Kahn, A. Tamayol, E. Arab-Tehrany, Bioact. Mater. 6 (2021) 3904–3923.
[42] J. Malda, J. Visser, F.P. Melchels, T. Jüngst, W.E. Hennink, W.J. Dhert, J. Groll, D. W. Hutmacher, Adv. Mater. 25 (2013) 5011–5028.
[43] K. Navindaran, J.S. Kang, K. Moon, J. Mech. Behav. Biomed. Mater. (2022) 105575.
[44] G. Singh, A. Chanda, Biomed. Mater. 16 (2021) 062004.
[45] C.F. Guimarães, L. Gasperini, A.P. Marques, R.L. Reis, Nat. Rev. Mater. 5 (2020) 351–370.
[46] Z. Qiao, J. Parks, P. Choi, H.-F. Ji, Polymers 11 (2019) 1773.
[47] S.K. Singh, Bioresour. Technol. Rep. (2022) 100958.